A REDUCED-ORDER MODELING TECHNIQUE FOR MISTUNED BLADED DISKS

Gisli Óttarsson*
Matthew P. Castanier**
Christophe Pierre†

The University of Michigan
Department of Mechanical Engineering and Applied Mechanics
Ann Arbor, Michigan 48109-2125

Abstract

The analysis of the response statistics of mistuned turbomachinery rotors requires an expensive Monte Carlo simulation approach. Simple lumped parameter models capture basic localization effects but do not represent well actual engineering structures without a difficult parameter identification. Current component mode analysis techniques generally require a minimum number of degrees of freedom which is too large for running Monte Carlo simulations at a reasonable cost. In the present work, a novel order reduction method is introduced which is capable of generating reasonably accurate, very low order models of bladed disks. This technique is based on component modes of vibration found from a finite element analysis of a single disk-blade sector.

1. Introduction

A system which features spatial repetition is known as a *periodic system*. A periodic system is an assembly of identical subsystems which are dynamically coupled in an identical manner. It is characterized by mode shapes which are extended throughout the system.

A periodic system is an idealization, however, since in an actual engineering structure, the substructures are not identical. Material and manufacturing flaws, as well as non-uniform wear and other operational factors, cause differences among the substructures. In some cases, these discrepancies, which are known as *disorder* or *mistuning*, can lead to localized mode shapes. Localized mode shapes feature large vibration amplitudes in a small region of the structure, with a spatial amplitude decay away from this region. This decay is asymptotically exponential over many realizations of a randomly mistuned structure. Localization is known to be especially severe in systems which feature weak coupling between subsystems [1].

* Graduate Student Research Assistant
Student member AIAA, ASME

** Graduate Student Research Assistant
Student member AIAA, ASME

† Associate Professor
Member AIAA, ASME

One group of structures which exhibit localization phenomena are turbomachinery rotors. Indeed, much of the early work in localization focused on turbomachinery [2, 3, 4, 5, 6]. Ideally, bladed disks in turbomachinery are cyclically symmetric, which means that they have rotational periodicity. One substructure would consist of a disk sector and one attached blade. In finite element models (FEMs) of bladed disks, modelers typically take advantage of cyclic symmetry by modeling only one disk-blade sector, and then finding the modes for the entire structure by applying a cyclicity argument. As a result, computation time and storage requirements are greatly reduced. Many finite element packages include cyclic symmetry routines for this purpose.

Since actual turbomachinery rotors feature mistuned blades, they often exhibit localized modes. Also, it is not uncommon for a rotor to have weak blade-to-blade coupling through the disk, which leads to strong localization. The attendant increase in forced response vibration amplitudes can cause rogue blades. Thus, there are great benefits to accurately modeling the structure and predicting localization effects. However, mistuning in the blades destroys the rotational periodicity, and therefore cyclic symmetry techniques cannot be employed. This means that the entire bladed disk must be modeled, which makes FEMs very expensive. In addition, mistuning is a random phenomenon, and many realizations of randomly mistuned structures must be run in Monte Carlo simulations or similar methods in order to predict localization. This makes FEMs impractical for mistuning analyses.

Reduced-order models (ROMs) of rotors have been developed so that localization may be studied. An example of a ROM is a lumped parameter model in which each disk sector is represented by a spring-mass oscillator that is connected to ground and coupled to neighboring sectors by linear springs, with the blades appearing as oscillators connected to each disk sector [7]. This model may be made more sophisticated by representing the disk sector or blade with multi-degree-of-freedom oscillators, or by allowing coupling to sectors other than the nearest neighboring sectors. Another type of model was introduced by Kaza and Kielb [8], in which the disk was modeled as a circular plate with constant thickness, and the blades were modeled by elastic beams. The blades were attached to the disk by maintaining continuity of displacement and slope at the disk-blade junction. The dynamics were described by the standing wave modes of the disk and the

traveling wave modes of the blades.

Such models capture the basic bladed disk dynamics, and exhibit localization due to mistuning. The localization may then be analyzed by using Monte Carlo techniques to determine the structure's sensitivity to localization for a given mistuning strength, by investigating the effect of various parameters on the localization, or by other types of analysis. However, in terms of representing actual systems, these models are rather crude. Furthermore, if one wishes to use such a model to predict the localization in a particular engineering structure, parameter identification can be extremely difficult.

There is therefore a need for an improved, systematic reduced-order modeling technique for bladed disks. Ideally, this technique would make use of a modal analysis for a single sector FEM, so that the ROM would represent well the actual structure. Furthermore, it should employ a component mode approach, with the disk and blades as the components, so that the blades' natural frequencies may be individually mistuned. Finally, the technique should be able to produce a model with a highly reduced number of degrees of freedom, so that Monte Carlo simulations may be performed at a reasonable cost.

Several component-mode modeling techniques exist [8, 9, 10, 11, 12], where the motion of the structure is described by a truncated set of component modes. However, none of these meet all of the requirements outlined above. In particular, most of these techniques require an additional set of mode shapes which allow the model to span the space of possible motions of the connected structure. These additional mode shapes are typically necessitated by artificial constraints imposed at component interfaces, and are therefore often referred to as *constraint modes*. The constraint modes can lead to an unsatisfactorily large number of degrees of freedom in the ROM. For instance, if one were to apply the Craig-Bampton technique to a solid element FEM, there would be 3 constraint modes for each finite element node at the disk-blade interface.

In this paper, we present a reduced-order modeling technique which is tailored to representing particular mistuned bladed disk structures based on a FEM of a single disk-blade sector of the tuned structure. We use a component-mode approach, in which the disk motion is described by finite element mode shapes of the disk, and the blade elastic motion is described by the finite element mode shapes of a blade fixed at the disk-blade interface. The motion of the blade due to the motion of the disk is described as a summation of disk mode motions at the disk-blade interface. Therefore, disk-blade attachment is achieved, and no constraint mode shapes are necessary. This technique:

- is systematic from the FEM of one disk-blade sector
- features the blade modal stiffnesses as explicit parameters so that the blade natural frequencies may be directly mistuned
- minimizes storage requirements
- is capable of producing models with a small number of degrees of freedom

This method places importance on the last item, and as a result it may not be as accurate as other component-mode techniques. However, with the present method, we can generate models which are of sufficiently low order as to be suitable for Monte Carlo simulations.

The paper is organized as follows. In section 2, we review the modes of cyclic systems, and formulate the equations of motion for the ROM. In addition, mistuning in the model is considered, and we explore the relationship between the present ROM and previous lumped parameter models as well as the associated transfer matrix method of analysis. In section 3, we describe in detail how the necessary mode shapes are generated from the FEM. We then present an example in section 4, using a simple FEM of one sector of the bladed disk. This system is represented by a full mistuned FEM in section 5, for the purposes of comparing the localized modes of the reduced-order and finite element models. We draw conclusions from this study in section 6.

2. Methodologies

In the vibration analysis of turbomachinery rotors it is normal to assume perfect cyclic symmetry, thereby reducing the analysis to that of one blade and the corresponding disk sector. In the first part of this section, the theory behind this type of analysis is briefly reviewed.

When the random mistuning of blade frequencies is considered, the cyclic symmetry assumption is no longer valid, requiring Monte Carlo simulations of models of the entire assembly. The second part of this section introduces an aggressive order reduction technique aimed at alleviating the cost of such analyses.

2.1. Cyclic Symmetry

Consider the finite element analysis of the free response of a structure with perfect cyclic symmetry.

$$\left[\mathbf{K} - \omega^2 \mathbf{M}\right]\mathbf{x} = \mathbf{0}$$

Assuming an identical element mesh for each disk-blade sector then the stiffness matrix, **K**, and the mass matrix, **M**, will have a *block circulant*, symmetric structure

$$\left(\begin{bmatrix} \mathbf{K}_o & \mathbf{K}_1 & \mathbf{K}_2 & \dots & \mathbf{K}_2 & \mathbf{K}_1 \\ \mathbf{K}_1 & \mathbf{K}_o & \mathbf{K}_1 & \dots & \mathbf{K}_3 & \mathbf{K}_2 \\ \mathbf{K}_2 & \mathbf{K}_1 & \mathbf{K}_o & \dots & \mathbf{K}_4 & \mathbf{K}_3 \\ \vdots & \vdots & \vdots & \ddots & \vdots & \vdots \\ \mathbf{K}_2 & \mathbf{K}_3 & \mathbf{K}_4 & \dots & \mathbf{K}_o & \mathbf{K}_1 \\ \mathbf{K}_1 & \mathbf{K}_2 & \mathbf{K}_3 & \dots & \mathbf{K}_1 & \mathbf{K}_o \end{bmatrix} - \omega^2 \begin{bmatrix} \mathbf{M}_o & \mathbf{M}_1 & \mathbf{M}_2 & \dots & \mathbf{M}_2 & \mathbf{M}_1 \\ \mathbf{M}_1 & \mathbf{M}_o & \mathbf{M}_1 & \dots & \mathbf{M}_3 & \mathbf{M}_2 \\ \mathbf{M}_2 & \mathbf{M}_1 & \mathbf{M}_o & \dots & \mathbf{M}_4 & \mathbf{M}_3 \\ \vdots & \vdots & \vdots & \ddots & \vdots & \vdots \\ \mathbf{M}_2 & \mathbf{M}_3 & \mathbf{M}_4 & \dots & \mathbf{M}_o & \mathbf{M}_1 \\ \mathbf{M}_1 & \mathbf{M}_2 & \mathbf{M}_3 & \dots & \mathbf{M}_1 & \mathbf{M}_o \end{bmatrix}\right) \begin{bmatrix} \mathbf{x}_1 \\ \mathbf{x}_2 \\ \mathbf{x}_3 \\ \vdots \\ \mathbf{x}_{N-1} \\ \mathbf{x}_N \end{bmatrix} = \mathbf{0} \tag{1}$$

where the block matrices $\mathbf{K}_i$ and $\mathbf{M}_i$ ($i = 0, \ldots, \mathrm{INT}[N/2]$) are square matrices of dimension equal to the number of degrees of freedom of each disk-blade sector.

All circulant matrices of dimension N share the same set of eigenvectors that are arranged as the columns of the Fourier matrix, **E**:

$$e_{ki} = \frac{1}{\sqrt{N}} e^{j2\pi(i-1)(k-1)/N}, \qquad i,k = 1,\ldots,N \qquad (j = \sqrt{-1}) \tag{2}$$

The **E** matrix is unitary, *i.e.*, $\mathbf{E}^*\mathbf{E} = \mathbf{I}$ where $*$ denotes the complex conjugate transpose. The Fourier matrix has a real valued form, **F**:

$$f_{ki} = \begin{cases} \dfrac{1}{\sqrt{N}} & \text{if } i = 1 \\ \sqrt{\dfrac{2}{N}} \cos \dfrac{2\pi(i-1)(k-1)}{N} & \text{if } 1 < i < \frac{N+2}{2} \\ \dfrac{(-1)^{k-1}}{\sqrt{N}} & \text{if } i = \frac{N+2}{2} \\ \sqrt{\dfrac{2}{N}} \sin \dfrac{2\pi(i-1)(k-1)}{N} & \text{if } \frac{N+2}{2} < i \le N \end{cases} \tag{3}$$

Note that the column $i = \frac{N+2}{2}$ only occurs if the number of blades, N, is even. The **F** matrix is orthogonal, *i.e.*, $\mathbf{F}^T\mathbf{F} = \mathbf{I}$.

Given this information, we see that Eq. (1) may be brought into a block diagonal form using the transformation

$$\mathbf{x} = (\mathbf{F} \otimes \mathbf{I})\,\mathbf{a}. \tag{4}$$

where $\otimes$ denotes the Kronecker product which is discussed in Appendix A. Thus

$$\left(\begin{bmatrix} \tilde{\mathbf{K}}_o & 0 & 0 & \ldots & 0 & 0 \\ 0 & \tilde{\mathbf{K}}_1^C & 0 & \ldots & 0 & 0 \\ 0 & 0 & \tilde{\mathbf{K}}_2^C & \ldots & 0 & 0 \\ \vdots & \vdots & \vdots & \ddots & \vdots & \vdots \\ 0 & 0 & 0 & \ldots & \tilde{\mathbf{K}}_2^S & 0 \\ 0 & 0 & 0 & \ldots & 0 & \tilde{\mathbf{K}}_1^S \end{bmatrix} - \omega^2 \begin{bmatrix} \tilde{\mathbf{M}}_o & 0 & 0 & \ldots & 0 & 0 \\ 0 & \tilde{\mathbf{M}}_1^C & 0 & \ldots & 0 & 0 \\ 0 & 0 & \tilde{\mathbf{M}}_2^C & \ldots & 0 & 0 \\ \vdots & \vdots & \vdots & \ddots & \vdots & \vdots \\ 0 & 0 & 0 & \ldots & \tilde{\mathbf{M}}_2^S & 0 \\ 0 & 0 & 0 & \ldots & 0 & \tilde{\mathbf{M}}_1^S \end{bmatrix} \right) \begin{bmatrix} \mathbf{a}_o \\ \mathbf{a}_1^C \\ \mathbf{a}_2^C \\ \vdots \\ \mathbf{a}_2^S \\ \mathbf{a}_1^S \end{bmatrix} = \mathbf{0} \tag{5}$$

thereby decoupling the many circumferential harmonics of the problem. For example, cosine modes of harmonic 2 (two nodal diameter modes) may be found by solving

$$\left(\tilde{\mathbf{K}}_2^C - \omega^2 \tilde{\mathbf{M}}_2^C\right) \mathbf{a}_2^C = 0 \tag{6}$$

This effectively reduces the size of the problem to that of only one sector. Many modern finite element codes feature this type of analysis.

2.2. ROMs of Nearly Cyclic Blade Assemblies

When blade mistuning prevents the use of cyclic symmetry arguments, a model of the full assembly is required. If the FEM is not given a much coarser mesh, the increase in problem size may be so drastic that the problem is rendered unsolvable. Furthermore, a full analysis of the statistics of response of a randomly mistuned system calls for multiple realizations of mistuned assemblies, which necessitates an even more severe order reduction. A full blown Monte Carlo simulation of a mistuned structure may require thousands of realizations, which is a monumental task unless the number of degrees of freedom per realization is kept within reason. In many cases, this may limit the number of degrees of freedom per sector to less than ten. Only modal analysis provides satisfactory accuracy at such low orders, and given the readily available modes of free vibration of the tuned assembly, a modal analysis of the mistuned problem is very tempting. However, in the modal analysis, all information about the blade dynamics is embedded in the modes, leaving no way of entering blade mistuning in a controlled manner.

An alternative approach is that of component mode analysis, in which the blades and the disk are treated as separate components. The most difficult problem in component mode analysis is the modeling of the interface between the components. This problem is effectively addressed in the several component mode techniques that have been suggested. Common to all of these techniques is the considerable expense associated with the assembly of the substructures, which for solid models adds three degrees of freedom for each node of the substructure interface. This cost is unacceptable for the analysis suggested herein. Instead, we consider the following simplified approach.

2.2.1. Nomenclature

N The number of disk-blade sectors.

P The maximum number of nodal diameters for a disk mode shape. $P = \mathrm{int}[N/2]$.

$\tilde{\mathbf{V}}_n$ A matrix formed with the selected n nodal diameter (n^{th} harmonic) mode shapes of the disk as its columns. The tilde signifies that each mode only contains the degrees of freedom of a single sector. When selecting modes to be considered in the analysis, both modes of a pair corresponding to a double natural frequency must be included. Note that the following analysis assumes that the vectors are normalized with respect to the mass matrix.

$\tilde{\mathbf{U}}_n^d$ Each column of this matrix is the disk-induced motion of a single blade when the disk sector to which it is attached is vibrating in a mode shape of $\tilde{\mathbf{V}}_n$. The ordering of these modes should correspond to $\tilde{\mathbf{V}}_n$. The scaling of these modes follows from the normalization of the modes of $\tilde{\mathbf{V}}_n$.

$\tilde{\mathbf{U}}^b$ A matrix formed with the selected set of cantilevered blade mode shapes as its columns.

$\otimes$ The Kronecker product (see Appendix A).

$\mathbf{V}_n$ The n nodal diameter mode shapes of an entire disk, formed by expanding the single sector mode shapes contained in $\tilde{\mathbf{V}}_n$, as explained in Appendix B.

$\mathbf{V}$ The matrix of all disk modes. $\mathbf{V} = [\mathbf{V}_0, \mathbf{V}_1, \ldots, \mathbf{V}_P]$

$\mathbf{U}_n^d$ Disk-induced motions of all the attached blades as the disk vibrates with the shapes in $\mathbf{V}_n$. The columns of $\mathbf{U}_n^d$ are formed like the columns of $\mathbf{V}_n$ (see Appendix B).

$\mathbf{U}^d$ The matrix of all disk-induced motions corresponding to $\mathbf{V}$. $\mathbf{U}^d = [\mathbf{U}_0^d, \mathbf{U}_1^d, \ldots, \mathbf{U}_P^d]$

$\mathbf{U}^b$ A block diagonal matrix, $\mathbf{U}^b = \left(\mathbf{I} \otimes \tilde{\mathbf{U}}^b\right)$, where the order of $\mathbf{I}$ is equal to N. Each block corresponds to the cantilevered mode shapes for an individual blade in the bladed disk.

$\mathbf{a}_n$ A vector of generalized coordinates corresponding to the n nodal diameter disk modes.

$\mathbf{a}$ The vector of generalized coordinates for all disk modes, $\mathbf{a} = [\mathbf{a}_0^T, \mathbf{a}_1^T, \ldots, \mathbf{a}_P^T]^T$

$\mathbf{b}_i$ A vector of generalized coordinates for blade i.

$\mathbf{b}$ The vector of generalized coordinates for all N blades. It is formed as $\mathbf{b} = \left[\mathbf{b}_1^T, \mathbf{b}_2^T, \ldots, \mathbf{b}_N^T\right]^T$.

$\mathbf{v}$ The disk deflection vector.

$$\mathbf{v} = \sum_{n=0}^{P} \mathbf{V}_n \mathbf{a}_n \tag{7}$$

$\mathbf{u}$ The blade deflection vector, containing the total motion of all N attached blades.

$$\mathbf{u} = \sum_{n=0}^{P} \mathbf{U}_n^d \mathbf{a}_n + \mathbf{U}^b \mathbf{b} \tag{8}$$

$\tilde{\mathbf{M}}_d, \tilde{\mathbf{K}}_d$ The finite element mass matrix and stiffness matrix of a disk sector.

$\mathbf{M}_d, \mathbf{K}_d$ The finite element mass matrix and stiffness matrix of the entire disk.

$\mathbf{I}, \hat{\mathbf{K}}_d$ The modal mass matrix and modal stiffness matrix of the entire disk. The modal mass matrix is the identity matrix since the modes are normalized with respect to the mass matrix.

$\tilde{\mathbf{M}}_b, \tilde{\mathbf{K}}_b$ The finite element mass matrix and stiffness matrix of a free blade.

$\mathbf{I}, \hat{\mathbf{K}}_b$ The modal mass matrix and modal stiffness matrix of a cantilevered blade with no mistuning. For simplicity, we choose the convention that blade mistuning only occurs in the blade modal stiffness matrix, and that the modal stiffness matrix of mistuned blade i is $\hat{\mathbf{K}}_b^i = (1+\delta_i)\hat{\mathbf{K}}_b$, where δ_i is a mistuning value from a random variable.

2.2.2. Formulation

The disk motion is written in terms of modal amplitudes, $\mathbf{Va}$ (see the Nomenclature section). The motion of an individual blade then consists of two components: the motion of the blade due to the disk motion, $\mathbf{U}^d\mathbf{a}$; and an elastic blade motion written in terms of a the modes of a cantilevered blade, $\mathbf{U}^b\mathbf{b}$. Since the elastic motion of the blade is written relative to the disk-induced motion of the blade, the attachment of the blade to the disk is automatic. Note that the disk-induced motion of the blade is *not* simply a rigid body motion, since it also accounts for the deformation of the blade due to disk deformation. Later sections explain how the modes in $\mathbf{V}$, $\mathbf{U}^b$, and $\mathbf{U}^d$ may be efficiently calculated with a finite element approach.

The kinetic energy of the assembly may be written as:

$$\begin{aligned}
T &= \frac{1}{2}\dot{\mathbf{v}}^T\mathbf{M}_d\dot{\mathbf{v}} + \frac{1}{2}\dot{\mathbf{u}}^T\mathbf{M}_b\dot{\mathbf{u}} \\
&= \frac{1}{2}\sum_{n=0}^{P}\left\{\dot{\mathbf{a}}_n^T\mathbf{V}_n^T\right\}\mathbf{M}_d\sum_{m=0}^{P}\{\mathbf{V}_m\dot{\mathbf{a}}_m\} \\
&\quad + \frac{1}{2}\left[\mathbf{U}^b\dot{\mathbf{b}} + \sum_{n=0}^{P}\mathbf{U}_n^d\dot{\mathbf{a}}_n\right]^T\mathbf{M}_b\left[\mathbf{U}^b\dot{\mathbf{b}} + \sum_{m=0}^{P}\mathbf{U}_m^d\dot{\mathbf{a}}_m\right] \\
&= \frac{1}{2}\sum_{n=0}^{P}\dot{\mathbf{a}}_n^T\dot{\mathbf{a}}_n + \frac{1}{2}\dot{\mathbf{b}}^T\dot{\mathbf{b}} + \dot{\mathbf{b}}^T\mathbf{U}^{bT}\mathbf{M}_b\sum_{n=0}^{P}\left\{\mathbf{U}_n^d\dot{\mathbf{a}}_n\right\} \\
&\quad + \frac{1}{2}\sum_{n=0}^{P}\left\{\dot{\mathbf{a}}_n^T\mathbf{U}_n^{dT}\right\}\mathbf{M}_b\sum_{m=0}^{P}\left\{\mathbf{U}_m^d\dot{\mathbf{a}}_m\right\}
\end{aligned} \tag{9}$$

Similarly, the strain energy is

$$\begin{aligned}
U &= \frac{1}{2}\mathbf{v}^T\mathbf{K}_d\mathbf{v} + \frac{1}{2}\mathbf{u}^T\mathbf{K}_b\mathbf{u} \\
&= \frac{1}{2}\sum_{n=0}^{P}\left\{\mathbf{a}_n^T\mathbf{V}_n^T\right\}\mathbf{K}_d\sum_{m=0}^{P}\{\mathbf{V}_m\mathbf{a}_m\} \\
&\quad + \frac{1}{2}\left[\mathbf{U}^b\mathbf{b} + \sum_{n=0}^{P}\mathbf{U}_n^d\mathbf{a}_n\right]^T\mathbf{K}_b\left[\mathbf{U}^b\mathbf{b} + \sum_{m=0}^{P}\mathbf{U}_m^d\mathbf{a}_m\right] \\
&= \frac{1}{2}\sum_{n=0}^{P}\mathbf{a}_n^T\hat{\mathbf{K}}_{dn}\mathbf{a}_n + \frac{1}{2}\mathbf{b}^T\mathbf{U}^{bT}\mathbf{K}_b\mathbf{U}^b\mathbf{b} \\
&\quad + \mathbf{b}^T\mathbf{U}^{bT}\mathbf{K}_b\sum_{n=0}^{P}\left\{\mathbf{U}_n^d\mathbf{a}_n\right\} \\
&\quad + \frac{1}{2}\sum_{n=0}^{P}\left\{\mathbf{a}_n^T\mathbf{U}_n^{dT}\right\}\mathbf{K}_b\sum_{m=0}^{P}\left\{\mathbf{U}_m^d\mathbf{a}_m\right\}
\end{aligned} \tag{10}$$

where $\hat{\mathbf{K}}_{dn}$ is the block of $\mathbf{K}_d$ which contains the modal stiffnesses of the disk modes with n nodal diameters. Recall that $\mathbf{U}^d$ constitutes the blade motions due to disk motion. It is clear that in many cases, this will be almost pure rigid body motion. It is our contention that the strain energy due to this term may often be negligible. It will, however, be included here.

We apply Hamilton's principle,

$$\int_{t_1}^{t_2} [\delta U - \delta T]\, dt = 0 \tag{11}$$

and find

$$\delta \mathbf{a}_n: \quad \ddot{\mathbf{a}}_n + \mathbf{U}_n^{dT}\mathbf{M}_b \sum_{m=0}^{P} \mathbf{U}_m^d \ddot{\mathbf{a}}_m + \mathbf{U}_n^{dT}\mathbf{M}_b\mathbf{U}^b\ddot{\mathbf{b}} + \hat{\mathbf{K}}_{dn}\mathbf{a}_n + \mathbf{U}_n^{dT}\mathbf{K}_b\mathbf{U}^b\mathbf{b} + \mathbf{U}_n^{dT}\mathbf{K}_b \sum_{m=0}^{P} \mathbf{U}_m^d \mathbf{a}_m = 0 \tag{12}$$

$$\delta \mathbf{b}: \quad \ddot{\mathbf{b}} + \sum_{n=0}^{P} \mathbf{U}^{bT}\mathbf{M}_b\mathbf{U}_n^d\ddot{\mathbf{a}}_n + \sum_{n=0}^{P} \mathbf{U}^{bT}\mathbf{K}_b\mathbf{U}_n^d\mathbf{a}_n + \left(\mathbf{diag}(1+\delta_i)\otimes\hat{\mathbf{K}}_b\right)\mathbf{b} = 0 \tag{13}$$

At this point we make an important approximation. Recall that we suggested above that the strain energy due to the disk-induced motion of the blade should in many cases be a small term. Given this assumption we elect to ignore the effect of blade mistuning in this term reasoning that the effect of mistuning on this small term will be negligible. Hence, blade mistuning will only be included in the strain energy of the blades due to the deformation of blades in the cantilevered blades modes. This approximation dramatically increases the efficiency of the generation of the reduced order equations of motion of the mistuned assembly.

We using the definition of $\mathbf{a}$ and $\mathbf{U}^d$ (see Nomenclature section) we may cast our equations into the following matrix form

$$\begin{bmatrix} \mathbf{I}+\mathbf{Bdiag}\left(\tilde{\mathbf{U}}_n^{dT}\tilde{\mathbf{M}}_b\tilde{\mathbf{U}}_n^d\right) & \mathbf{U}^{dT}\mathbf{M}_b\mathbf{U}^b \\ \mathbf{U}^{bT}\mathbf{M}_b\mathbf{U}^d & \mathbf{I} \end{bmatrix}\begin{bmatrix}\ddot{\mathbf{a}}\\ \ddot{\mathbf{b}}\end{bmatrix} + \begin{bmatrix} \hat{\mathbf{K}}_d+\mathbf{Bdiag}\left(\tilde{\mathbf{U}}_n^{dT}\tilde{\mathbf{K}}_b\tilde{\mathbf{U}}_n^d\right) & \mathbf{U}^{dT}\mathbf{K}_b\mathbf{U}^b \\ \mathbf{U}^{bT}\mathbf{K}_b\mathbf{U}^d & \mathbf{diag}(1+\delta_i)\otimes\hat{\mathbf{K}}_b \end{bmatrix}\begin{bmatrix}\mathbf{a}\\ \mathbf{b}\end{bmatrix} = \mathbf{0} \tag{14}$$

where **Bdiag** denotes a block diagonal matrix, and **diag** denotes a diagonal matrix. A few comments about Eq. (14) are in order. First it is to be noted that no information about mode shapes in the disk is required. Only the modal stiffnesses of the disk and blade modes, the disk-induced shape functions and elastic modes in the blade, and the blade mass and stiffness matrices enter the analysis.

In the mass and stiffness matrices, the bottom right blocks are diagonal, *i.e.*, no coupling of blade modes occurs. Coupling of blade modes and disk modes appears in the top right and bottom left blocks of the mass and stiffness matrices. These blocks are in general full, hence there is full coupling of all blade and disk modes. The top left blocks feature two terms: one that corresponds to the disk alone, and a second term related to the assembly of disk and blades. Yet, we note that the top left blocks of the mass and stiffness matrices are block diagonal for the following reason: addition of blade inertia preserves the cyclicity of the assembly. Likewise, since the contribution of blade stiffness mistuning on the disk-induced strain energy in the blades was ignored, addition of blade stiffness does not alter the cyclicity of the disk. Hence there is no coupling among the different nodal diameter modes. However, the addition of the blade inertia and stiffness couples the modal circle modes that have the same number of nodal diameters.

An examination of Eq. (14) reveals the reason for ignoring the contribution of blade stiffness mistuning on the disk-induced strain energy. Thanks to this approximation, the mistuning random variables δ_i only appear in the bottom right hand block, which is the only block that must be generated for successive mistuning patterns. If this assumption had not been made, the entire stiffness matrix would have to be regenerated for each mistuning pattern.

As an aside, we point out the fact that individual blades are not directly coupled. Thus, the blade degrees of freedom may be written in terms of disk coordinates. This is strictly equivalent to the elimination of all degrees of freedom except the coupling coordinates that was shown to be possible in the coupled oscillator models [13]. From Eq. (13), assuming harmonic motion,

$$\left[\mathbf{U}^{bT}\mathbf{K}_b\mathbf{U}^d - \omega^2\mathbf{U}_b^T\mathbf{M}_b\mathbf{U}^d\right]\mathbf{a} + \left[\mathbf{diag}(1+\delta_i)\otimes\hat{\mathbf{K}}_b - \omega^2\mathbf{I}\right]\mathbf{b} = 0 \tag{15}$$

where the matrix $\left[\mathbf{diag}(1+\delta_i)\otimes\hat{\mathbf{K}}_b - \omega^2\mathbf{I}\right]$ is diagonal. For this reason, the blade degrees of freedom may be efficiently represented in terms of the disk degrees of freedom. By substituting this relationship into Eq. (12), thereby eliminating $\mathbf{b}$ the computational efficiency may be greatly improved. However, this elimination of blade coordinates may be of limited use in a free response analysis, because the natural frequencies become embedded in the eigenvalue problem preventing the use of canned eigenvalue solvers. The elimination of blade degrees of freedom should considered an essential part of a forced response analysis or a transfer matrix approach.

2.2.3. Pseudo-Physical Coordinate System

The coordinate system presented above features a mixture of modal amplitudes of interblade phase angle modes for the disk, and blade modal amplitudes. Hence, only the blade degrees of freedom in the reduced order model are directly associated with individual sectors. Therefore, a direct comparison with the lumped mass

models hitherto utilized in the analysis of bladed disks is difficult. A coordinate transformation from the disk modal amplitude coordinates to disk sector coordinates would be useful.

Since the top left blocks of the mass and stiffness matrices are block diagonal, there exists a transformation to a block circulant form (See Eq. (4)). The resulting coordinate system will be referred to as *pseudo-physical* coordinates, because the transformation is to the deflections of an equivalent lumped mass model for the disk sector. The transformation does not effect the blade degrees of freedom. We define the following transformed matrices:

$$\mathbf{A} = (\mathbf{F}\otimes\mathbf{I})\left[\mathbf{I} + \mathbf{B}\mathrm{diag}\left(\tilde{\mathbf{U}}_n^{dT}\tilde{\mathbf{M}}_b\tilde{\mathbf{U}}_n^{d}\right)\right]\left(\mathbf{F}\otimes\mathbf{I}^T\right) \tag{16}$$

$$\mathbf{B} = (\mathbf{F}\otimes\mathbf{I})\left(\mathbf{U}^{dT}\mathbf{M}_b\mathbf{U}^{b}\right) \tag{17}$$

$$\mathbf{C} = (\mathbf{F}\otimes\mathbf{I})\left[\mathbf{I} + \mathbf{B}\mathrm{diag}\left(\tilde{\mathbf{U}}_n^{dT}\tilde{\mathbf{M}}_b\tilde{\mathbf{U}}_n^{d}\right)\right]\left(\mathbf{F}\otimes\mathbf{I}^T\right) \tag{18}$$

$$\mathbf{D} = (\mathbf{F}\otimes\mathbf{I})\left(\mathbf{U}^{dT}\mathbf{K}_b\mathbf{U}^{b}\right) \tag{19}$$

Eq. (14) may then be rewritten in the pseudo-physical coordinate basis as

$$\left[\begin{array}{c|c} \mathbf{A} & \mathbf{B} \\ \hline \mathbf{B}^T & \mathbf{I} \end{array}\right]\left[\begin{array}{c} \ddot{\mathbf{y}} \\ \ddot{\mathbf{b}} \end{array}\right] + \left[\begin{array}{c|c} \mathbf{C} & \mathbf{D} \\ \hline \mathbf{D}^T & \mathrm{diag}[\hat{\mathbf{K}}_i] \end{array}\right]\left[\begin{array}{c} \mathbf{y} \\ \mathbf{b} \end{array}\right] = \mathbf{0} \tag{20}$$

where $\mathbf{y}$ is the vector of disk pseudo-physical coordinates. We have introduced the notation $\mathbf{diag}[\hat{\mathbf{K}}_i]$ for the diagonal matrix of mistuned modal stiffnesses, $\mathbf{diag}(1+\delta_i)\otimes\hat{\mathbf{K}}_b$.

Equation (20) still features the inertial coupling of blades observed in Eq. (14), caused by the coordinate system for the blades being relative to the disk. Yet another step is required to complete the transformation to the lumped mass models similar to the ones in the literature which usually feature absolute deflections resulting in stiffness coupling of the blades.

We define a transformation from $\mathbf{b}$, the coordinates of blade motion relative to disk motion, to $\mathbf{z}$, the coordinates of absolute blade motion.

$$\mathbf{z} = \mathbf{B}^T\mathbf{y} + \mathbf{b} \tag{21}$$

Applying Eq. (21), Eq. (20) becomes

$$\left[\begin{array}{c|c} \mathbf{A}-\mathbf{B}\mathbf{B}^T & \mathbf{0} \\ \hline \mathbf{0} & \mathbf{I} \end{array}\right]\left[\begin{array}{c} \ddot{\mathbf{y}} \\ \ddot{\mathbf{z}} \end{array}\right] + \left[\begin{array}{c|c} \mathbf{B}\,\mathrm{diag}[\hat{\mathbf{K}}_i]\mathbf{B}^T+\mathbf{C} & \mathbf{D}-\mathbf{B}\,\mathrm{diag}[\hat{\mathbf{K}}_i] \\ \hline \mathbf{D}^T-\mathrm{diag}[\hat{\mathbf{K}}_i]\mathbf{B}^T & \mathrm{diag}[\hat{\mathbf{K}}_i] \end{array}\right]\left[\begin{array}{c} \mathbf{y} \\ \mathbf{z} \end{array}\right] = \mathbf{0} \tag{22}$$

which features the more familiar stiffness coupling of individual blades through the disk. Finally, $[\mathbf{y},\mathbf{z}]^T$ may be reordered so that coordinates of each sector are grouped. The vector $\mathbf{x}^T$ is formed, where $\mathbf{x}_i$ contains both blade and disk *absolute, pseudo-physical* coordinates of sector *i*. In a tuned form, the equations of motion have the form presented in Eq. (1). In the mistuned case, the circulant form of Eq. (1) is destroyed giving rise to the form

$$\left(\begin{bmatrix} \mathbf{K}_o^1 & \mathbf{K}_1^1 & \mathbf{K}_2^1 \dots \mathbf{K}_2^1 & \mathbf{K}_1^1 \\ \mathbf{K}_1^2 & \mathbf{K}_o^2 & \mathbf{K}_1^2 \dots \mathbf{K}_3^2 & \mathbf{K}_2^2 \\ \mathbf{K}_2^3 & \mathbf{K}_1^3 & \mathbf{K}_o^3 \dots \mathbf{K}_4^3 & \mathbf{K}_3^3 \\ \vdots & \vdots & \vdots\ddots\vdots & \vdots \\ \mathbf{K}_2^{N-1} & \mathbf{K}_3^{N-1} & \mathbf{K}_4^{N-1} \dots \mathbf{K}_o^{N-1} & \mathbf{K}_1^{N-1} \\ \mathbf{K}_1^N & \mathbf{K}_2^N & \mathbf{K}_3^N \dots \mathbf{K}_1^N & \mathbf{K}_o^N \end{bmatrix} - \omega^2 \begin{bmatrix} \mathbf{M}_o & \mathbf{M}_1 & \mathbf{M}_2 \dots \mathbf{M}_2 & \mathbf{M}_1 \\ \mathbf{M}_1 & \mathbf{M}_o & \mathbf{M}_1 \dots \mathbf{M}_3 & \mathbf{M}_2 \\ \mathbf{M}_2 & \mathbf{M}_1 & \mathbf{M}_o \dots \mathbf{M}_4 & \mathbf{M}_3 \\ \vdots & \vdots & \vdots\ddots\vdots & \vdots \\ \mathbf{M}_2 & \mathbf{M}_3 & \mathbf{M}_4 \dots \mathbf{M}_o & \mathbf{M}_1 \\ \mathbf{M}_1 & \mathbf{M}_2 & \mathbf{M}_3 \dots \mathbf{M}_1 & \mathbf{M}_o \end{bmatrix}\right)\begin{bmatrix} \mathbf{x}_1 \\ \mathbf{x}_2 \\ \mathbf{x}_3 \\ \vdots \\ \mathbf{x}_{N-1} \\ \mathbf{x}_N \end{bmatrix} = \mathbf{0} \tag{23}$$

where the superscripts in the stiffness matrix correspond to the sector numbers.

2.2.4. Transfer Matrices

In the earlier work by the authors [7, 13], a transfer matrix approach to the analysis of bladed-disks was presented. A low number of coupling coordinates was shown the be the prerequisite to the applicability of this approach. It was hypothesized that in many cases the elements of M and K will exhibit rapid decay away from diagonal. In such cases, the dominance of the coupling between neighboring sectors may be capitalized upon by ignoring the coupling between weakly coupled sectors. Assume, for instance, that only three blocks away from the diagonal in Eq. (23) are deemed significant. Then the remaining blocks may be truncated and the dynamics of the system represented in a transfer matrix form

$$\begin{bmatrix} \mathbf{x}_{i+1} \\ \mathbf{x}_i \\ \mathbf{x}_{i-1} \\ \mathbf{x}_{i-2} \\ \mathbf{x}_{i-3} \\ \mathbf{x}_{i-4} \end{bmatrix} = \begin{bmatrix} -\mathbf{T}_1^i & -\mathbf{T}_2^i & -\mathbf{T}_3^i & -\mathbf{T}_2^i & -\mathbf{T}_1^i & -\mathbf{I} \\ \mathbf{I} & \mathbf{0} & \mathbf{0} & \mathbf{0} & \mathbf{0} & \mathbf{0} \\ \mathbf{0} & \mathbf{I} & \mathbf{0} & \mathbf{0} & \mathbf{0} & \mathbf{0} \\ \mathbf{0} & \mathbf{0} & \mathbf{I} & \mathbf{0} & \mathbf{0} & \mathbf{0} \\ \mathbf{0} & \mathbf{0} & \mathbf{0} & \mathbf{I} & \mathbf{0} & \mathbf{0} \\ \mathbf{0} & \mathbf{0} & \mathbf{0} & \mathbf{0} & \mathbf{I} & \mathbf{0} \end{bmatrix}\begin{bmatrix} \mathbf{x}_i \\ \mathbf{x}_{i-1} \\ \mathbf{x}_{i-2} \\ \mathbf{x}_{i-3} \\ \mathbf{x}_{i-4} \\ \mathbf{x}_{i-5} \end{bmatrix} \tag{24}$$

where

$$\mathbf{T}_1^i = \left(\mathbf{K}_3^i - \omega^2\mathbf{M}_3\right)^{-1}\left(\mathbf{K}_2^i - \omega^2\mathbf{M}_2\right)$$

$$\mathbf{T}_2^i = \left(\mathbf{K}_3^i - \omega^2\mathbf{M}_3\right)^{-1}\left(\mathbf{K}_1^i - \omega^2\mathbf{M}_1\right)$$

$$\mathbf{T}_3^i = \left(\mathbf{K}_3^i - \omega^2\mathbf{M}_3\right)^{-1}\left(\mathbf{K}_0^i - \omega^2\mathbf{M}_0\right)$$

Naturally, the elimination of the blade degrees of freedom as discussed above is highly advantageous since it reduces the dimension of the blocks of the transfer matrix.

3. Generating Component Modes Using the FEM

In this section we outline how the the finite element method may be utilized to obtain the ingredients required for the order reduction method. Two separate finite element eigenvalue analyses are required: a cyclic symmetry analysis of the disk alone, and an analysis of a fixed blade. Throughout the discussion it is assumed that eigenvectors are normalized with respect to the mass matrix. From Eq. (14) we make the following inventory:

- mode shapes for a fixed blade, $\tilde{\mathbf{U}}^b$
- corresponding modal stiffnesses, $\hat{\mathbf{K}}_b$
- the finite element mass and stiffness matrices of a free blade, $\tilde{\mathbf{M}}_b$ and $\tilde{\mathbf{K}}_b$
- shape functions for the attached blades that are due to nodal diameter mode shapes in the disk, $\tilde{\mathbf{U}}^d$
- modal stiffnesses of the disk nodal diameter modes, $\hat{\mathbf{K}}_d$

The eigenvalue analysis of a single cantilevered blade is straightforward. The blade mass and stiffness matrices may not be as easily obtained but are required for the analysis.

The method for obtaining the disk-induced shapes in the blade is less apparent. An approach fundamental to the current work is as follows. By performing the cyclic symmetry analysis of the disk component with *massless* blades attached, the required shape functions in the blade are automatically generated. This technique requires no modification to a pre-existing FEM apart from setting the blade material density to zero. Because massless blades have no inertia, they will follow the motion of the disk, and will not add spurious natural frequencies.

A serendipitous consequence of this approach is the stiffening of the disk component by the attached blades. Since this setup mimics the actual disk-blade interface, the disk mode shapes are improved. As a result modal convergence is enhanced. The analysis yields the desired number of *families* of nodal diameter modes for the disk component. A *family* refers to all nodal diameter modes of a certain type in the disk, *e.g.*, the one nodal circle out of plane bending. Only the modal stiffnesses of the modes as well as the part of the eigenvectors pertaining to the blade (the blade shape functions) are retained. The part of the eigenvectors pertaining to the disk (the disk modes) are discarded.

4. Example

As an example, we present a simple FEM of one sector of a fictitious bladed-disk structure. Top and side views of the finite element mesh are shown in Fig. 1. The elements are all eight-noded solid bricks. The disk sector has 15 elements, and the blade has 3 elements. In general, the blade substructure may be defined as the part of the model which is to have mistuned properties.

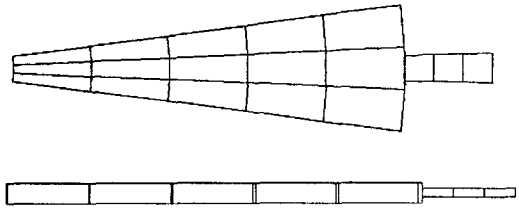

Figure 1 An example finite element model.

All nodes of the inner radius of the disk are completely constrained. Also, all elements have the same material properties. This FEM therefore represents a blisk which is clamped at the inner radius. There are 138 degrees of freedom per disk-blade sector, and a total of 24 sectors for the full blisk. All finite element work was done on NASTRAN using SOL 48 for the disk component, and SOL 103 for the cantilevered blade.

Although this model is simple, the properties and dimensions were chosen so that the dynamics would be quite challenging to reproduce with a ROM. As a benchmark, we show the natural frequencies of the FEM versus the number of nodal diameters in Fig. 2. Note that this plot shows several very close frequency veerings.

For the ROM, we take five families of disk modes, and four cantilevered elastic blade modes. Thus, there are *nine* degrees of freedom per sector for the ROM, compared to 138 degrees of freedom per sector for the FEM.

The natural frequencies found from the ROM are compared to the finite element frequencies in Fig. 3. Globally, the frequency distribution is very well captured by the ROM. In particular, the disk modes are almost exact. The blade modes are nicely approximated although not as accurately as the disk modes. The ROM frequencies for blade modes tend to be higher than the FEM frequencies. This is most likely due to the fact that cantilevered blade modes were used, and the fixed end boundary condition makes the blade modal stiffnesses too large. The low number of disk mode families accounted, for fails to compensate for this. The exaggerated stiffness is most apparent in the second blade mode.

It is especially gratifying to see the performance of the ROM in the neighborhood of the frequency curve veerings. The veerings are directly related to the disk-blade coupling (and therefore blade-to-blade coupling) which has been shown to be the single most inportant factor in the analysis of mode localization [1, 13]. This suggests that the proposed reduced order modeling technique will provide a valuable tool in the analysis of mistuning sensitivity in bladed disks.

The previous nine-degree-of-freedom model captures well the natural frequencies in a rather broad frequency range. For the purposes of mistuning analysis, however, the structural dynamicist often chooses to focus on a small frequency band which includes a set of blade modes. It is the blade modes which feature large localization, and are

therefore of primary importance. We now take the first two families of FEM disk modes and the first FEM blade mode in order to create a ROM with only *three* degrees of freedom per sector.

The natural frequencies of the ROM with three degrees of freedom are shown in Fig. 4. Considering that we have approximated a 138-degree-of-freedom-per-sector model with a three-degree-of-freedom-per-sector model, the frequency fit is excellent.

5. Mistuning

In order to reproduce the dynamics of the FEM with the ROM, not only must the frequencies be well approximated, but the mode shapes must match as well. Even though the *component* mode shapes for the ROM are taken from the FEM, we are interested in comparing the mode shapes for the bladed disk assembly, which are created in the reduced-order modeling process. In addition, we need to verify that the mistuning effects are well captured by the ROM. Therefore, we proceed to validate the order reduction method by examining how well the frequencies and the localized mode shapes of the ROM compare to those of the FEM for one realization of a mistuned bladed disk.

For this validation, we constructed a FEM for the full blisk of which one sector was presented in Fig. 1. Mistuning was added by allowing each blade to have a different Young's modulus. The Young's modulus for each blade i, E_i, was found as:

$$E_i = E_0(1 + \delta_i) \tag{25}$$

where E_0 is the Young's modulus for a tuned blade, and δ_i is a sample — from a uniform distribution with standard deviation 5% — produced by a random number generator.

For this mistuning example, we use the ROM with nine degrees of freedom per sector. The modal stiffnesses of the ROM were changed so that the mistuning pattern was identical to that of the FEM. Note that 5% stiffness mistuning corresponds to approximately 2.5% blade natural frequency mistuning. The FEM considered here has a total of 3312 degrees of freedom, while the ROM has only 216 degrees of freedom.

Since the mistuning destroys the cyclic symmetry of the structure, the modes will no longer be associated with a certain number of nodal diameters. We therefore plot the natural frequencies of both models versus occurrence number in Fig. 5. The frequencies of the two models compare very well over this frequency range. Note, however, that the frequencies of the in-plane blade modes are still higher for the ROM than for the FEM.

Finally, we compare selected localized mode shapes of the FEM and ROM in Fig. 6. The vibration amplitude of each blade was reduced to a scalar by taking the square root of the sum of the squares of the amplitudes for all degrees of freedom in the blade. The vector of these amplitudes was then normalized so as to have unit length.

Note that the mode shapes are very similar. Although the amplitudes at a certain blade may differ slightly, the maximum amplitudes occur at the same blade and are very close. Furthermore, the mode shapes of the FEM and ROM exhibit similar spatial amplitude decay, and we found this to be typical of the FEM and ROM modes. This is of primary importance since it demonstrates that the two models have comparable sensitivities to mistuning.

6. Conclusions

A reduced-order modeling technique was presented which is tailored to producing a very low-order model of an actual bladed disk structure. The method is systematic from a finite element model (FEM) of one disk-blade sector of the structure. A component mode approach is used, where the disk modal stiffnesses and the blade motion due to disk mode shapes are found from the FEM modes of the disk with *massless* blades. The blade modal stiffnesses are found from the FEM modes of the blade with all nodes at the disk-blade interface fixed. The finite element mass and stiffness matrices for the blade alone are also used. This is all the information that is needed from the FEM runs, so storage requirements are modest. Mistuning may easily be added to the reduced-order model (ROM) by slightly disordering the blade stiffness properties.

For the example case considered, the reduced-order modeling technique performed well. For order reduction per sector 138 → 9, the system dynamics were well captured over a broad frequency range. For order reduction per sector 138 → 3, the system natural frequencies were approximated in the frequency band of interest. It was found that the technique captures well blade-disk coupling, an important feature in the analysis of blade mistuning.

The frequencies and mode shapes were compared for the FEM and ROM of the example system with mistuned blade stiffnesses. The frequencies for the two models were very similar. The match between FEM and ROM mistuned mode shapes was excellent. The maximum amplitudes occurred at the same blade and were nearly equal in magnitude. Also, the spatial amplitude decay rates were similar, which means that sensitivity to mistuning is well preserved in the order reduction process.

References

[1] Hodges, C. H., "Confinement of Vibration by Structural Irregularity," *Journal of Sound and Vibration*, vol. 82, 1982, pp. 411-424.

[2] Dye, R. C. and Henry, T. A., "Vibration Amplitudes of Compressor Blades Resulting From Scatter in Blade Natural Frequencies," *ASME Journal of Engineering for Power*, vol. 91, 1969, pp. 182-188.

[3] El-Bayoumy, L. E. and Srinivasan, A. V., "Influence of Mistuning on Rotor-Blade Vibrations," *AIAA Journal*, vol. 13, no. 4, 1975, pp. 460-464.

[4] Ewins, D. J., "Vibration Modes of Mistuned Bladed Disks," *ASME Journal of Engineering for Power*, July 1976, pp. 349-355.
[5] Kaza, K. R. V. and Kielb, R. E., "Flutter and Response of a Mistuned Cascade in Incompressible Flow," *AIAA Journal*, vol. 20, no. 8, 1982, pp. 1120-1127.
[6] Bendiksen, O. O., "Flutter of Mistuned Turbomachinery Rotors," *ASME Journal of Engineering for Gas Turbines and Power*, vol. 106, no. 1, 1984, pp. 25-33.
[7] Ottarsson, G. S. and Pierre, C., "Vibration Localization in Mono- and Bi-Coupled Bladed Disks — A Transfer Matrix Approach," in *The Proceedings of the 34th AIAA/ASME/ASCE/AHS/ASC Structures, Structural Dynamics and Materials Conference*, vol. 6, (La Jolla, California), pp. 3683-3697, April 1993.
[8] Kaza, K. R. V. and Kielb, R. E., "Effects of Structural Coupling on Mistuned Cascade Flutter and Response," *ASME Journal of Engineering for Gas Turbines and Power*, vol. 106, no. 1, 1984, pp. 17-24.
[9] Hurty, W. C., "Dynamic Analysis of Structural Systems Using Component Modes," *AIAA Journal*, vol. 3, no. 4, 1965, pp. 678-685.
[10] Craig, R. R. and Bampton, M. C. C., "Coupling of Substructures for Dynamics Analyses," *AIAA Journal*, vol. 6, no. 7, 1968, pp. 1313-1319.
[11] Benfield, W. A. and Hruda, R. F., "Vibration Analysis of Structures by Component Mode Substitution," *AIAA Journal*, vol. 9, no. 7, 1971, pp. 1255-1261.
[12] Dowell, E. H., "Free vibrations of an arbitrary structure in terms of component modes," *ASME Journal of Applied Physics*, vol. 4, 1972, pp. 1145-1161.
[13] Ottarsson, G. S. and Pierre, C., "A Transfer Matrix Approach to Vibration Localization in Mistuned Blade Assemblies," in *The Proceedings of the International Gas Turbine and Aeroengine Congress*, no. 93-GT-115, (Cincinnati, Ohio), May 1993.

Appendix A: The Kronecker Product A⊗B

In the study of the block circulant matrices, that arise in the analysis of structures with cyclic symmetry, the Kronecker produce is a useful tool. A brief introduction of the product and some of its properties is in order. Many users will be be familiar with the Kronecker product of a column vector and a line vector to form a matrix

$$\mathbf{D} = \mathbf{a} \otimes \mathbf{b} = \begin{bmatrix} a_1 b_1 & a_1 b_2 & \dots & a_1 b_N \\ a_2 b_1 & a_2 b_2 & \dots & a_2 b_N \\ \vdots & \vdots & \ddots & \vdots \\ a_N b_1 & a_N b_2 & \dots & a_N b_N \end{bmatrix}$$

The Kronecker product of two matrices is

$$\mathbf{C} = \mathbf{A} \otimes \mathbf{B} = \begin{bmatrix} a_{11}\mathbf{B} & a_{12}\mathbf{B} & a_{13}\mathbf{B} & \dots \\ a_{21}\mathbf{B} & a_{22}\mathbf{B} & \dots & \dots \\ \vdots & \vdots & \ddots & \ddots \end{bmatrix}$$

Some of the useful properties of the Kronecker product include

$$(\mathbf{A} \otimes \mathbf{B})\,(\mathbf{C} \otimes \mathbf{D}) = (\mathbf{AC}) \otimes (\mathbf{BD})$$

$$(\mathbf{A} \otimes \mathbf{B})^* = \mathbf{A}^* \otimes \mathbf{B}^*$$

Appendix B: Generation of Full Assembly Mode Shapes

A finite element analysis of a blade assembly, using cyclic symmetry, yields the real and imaginary parts of an n^{th} harmonic mode of a single sector

$$\tilde{\mathbf{v}}_n = \tilde{\mathbf{v}}_n^R + j\tilde{\mathbf{v}}_n^I. \tag{26}$$

The corresponding pair of counter-rotating (complex conjugate) modes of the entire assembly may be generated using the Kronecker product (see Appendix A)

$$\hat{\mathbf{v}}_n = \mathbf{e}_n \otimes \tilde{\mathbf{v}}_n \tag{27}$$

and

$$\hat{\mathbf{v}}_n^* = \mathbf{e}_n^* \otimes \tilde{\mathbf{v}}_n^* \tag{28}$$

where $\mathbf{e}_n$ is the n^{th} harmonic vector from the Fourier matrix E in Eq. (2),

$$\mathbf{e}_n = \frac{1}{\sqrt{N}} \begin{bmatrix} 1 \\ \cos\sigma_n + j\sin\sigma_n \\ \vdots \\ \cos[(N-1)\sigma_n] + j\sin[(N-1)\sigma_n] \end{bmatrix}$$

Here, $\sigma = \frac{2\pi n}{N}$ is the interblade phase angle of the mode pair. We may write Eqs. (27) and (28) as

$$\hat{\mathbf{v}}_n\,,\, \hat{\mathbf{v}}_n^* = \left[\mathbf{f}_n^c \otimes \tilde{\mathbf{v}}_n^R - \mathbf{f}_n^s \otimes \tilde{\mathbf{v}}_n^I\right] \pm j\left[\mathbf{f}_n^s \otimes \tilde{\mathbf{v}}_n^R + \mathbf{f}_n^c \otimes \tilde{\mathbf{v}}_n^I\right].$$

where f_n^s and f_n^c denote, respectively the n^{th} harmonic sine and cosine vectors from the real form of the Fourier matrix F in Eq. (3). We may define a new pair of eigenvectors as the real and imaginary parts of $\hat{\mathbf{v}}_n$ and $\hat{\mathbf{v}}_n^n$,

$$\mathbf{v}_n^c = \left[\mathbf{f}_n^c \otimes \tilde{\mathbf{v}}_n^R - \mathbf{f}_n^s \otimes \tilde{\mathbf{v}}_n^I\right]$$

and

$$\mathbf{v}_n^s = \left[\mathbf{f}_n^s \otimes \tilde{\mathbf{v}}_n^R + \mathbf{f}_n^c \otimes \tilde{\mathbf{v}}_n^I\right].$$

All the modes of the blade assembly may be written in this form and put into a matrix $\mathbf{V} = [\mathbf{v}_0, \mathbf{v}_1^s, \mathbf{v}_1^c, \mathbf{v}_2^s, \mathbf{v}_2^c, \dots]$.

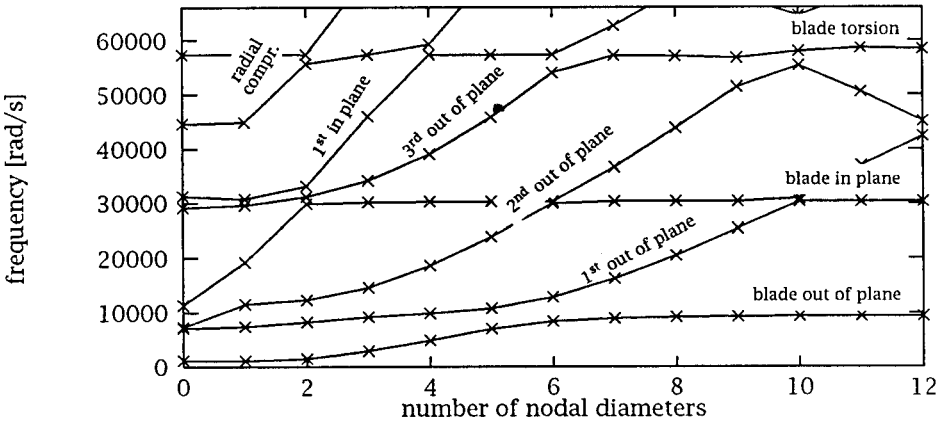

Figure 2 Natural frequencies of the example system shown as a function of the number of nodal diameters in the corresponding mode shape. The lines connect members of a modal families.

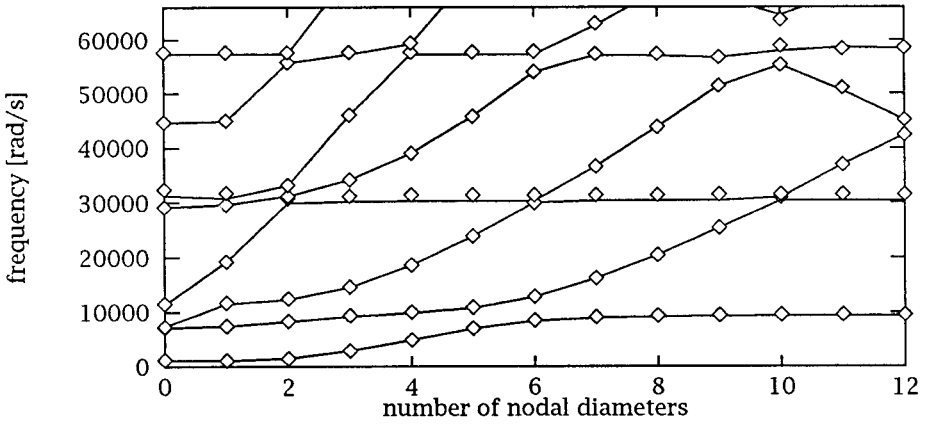

Figure 3 Natural frequencies of 9-degree-of-freedom ROM (◇) compare favorably with the natural frequencies of the FEM (—) when plotted as a function of the number of nodal diameters in the corresponding mode shape.

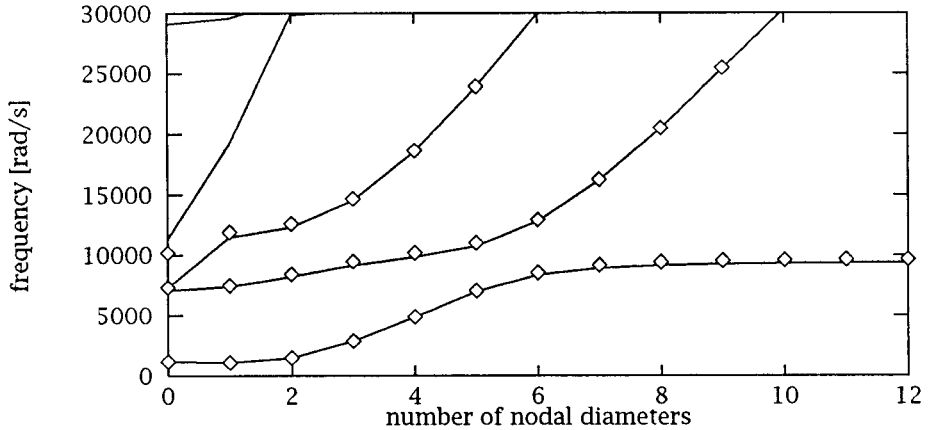

Figure 4 Natural frequencies of 3-degree-of-freedom ROM (◇) compare favorably with the natural frequencies of the FEM (—) in a narrow frequency band.

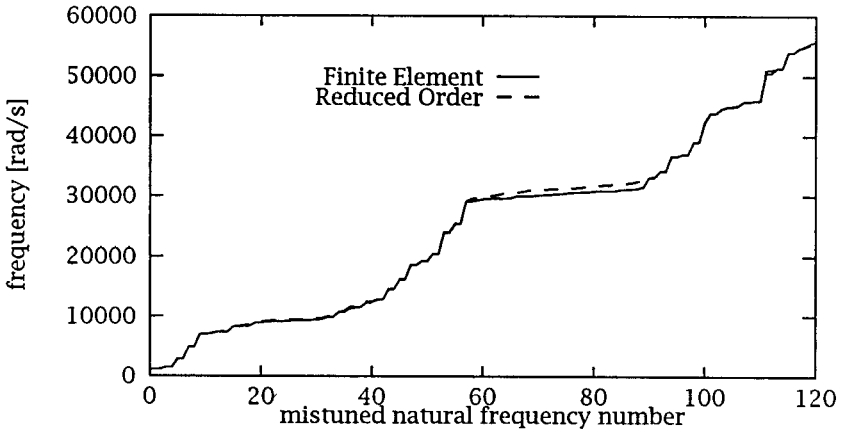

Figure 5 Comparison of the natural frequencies of the FEM and ROM for the mistuned case.

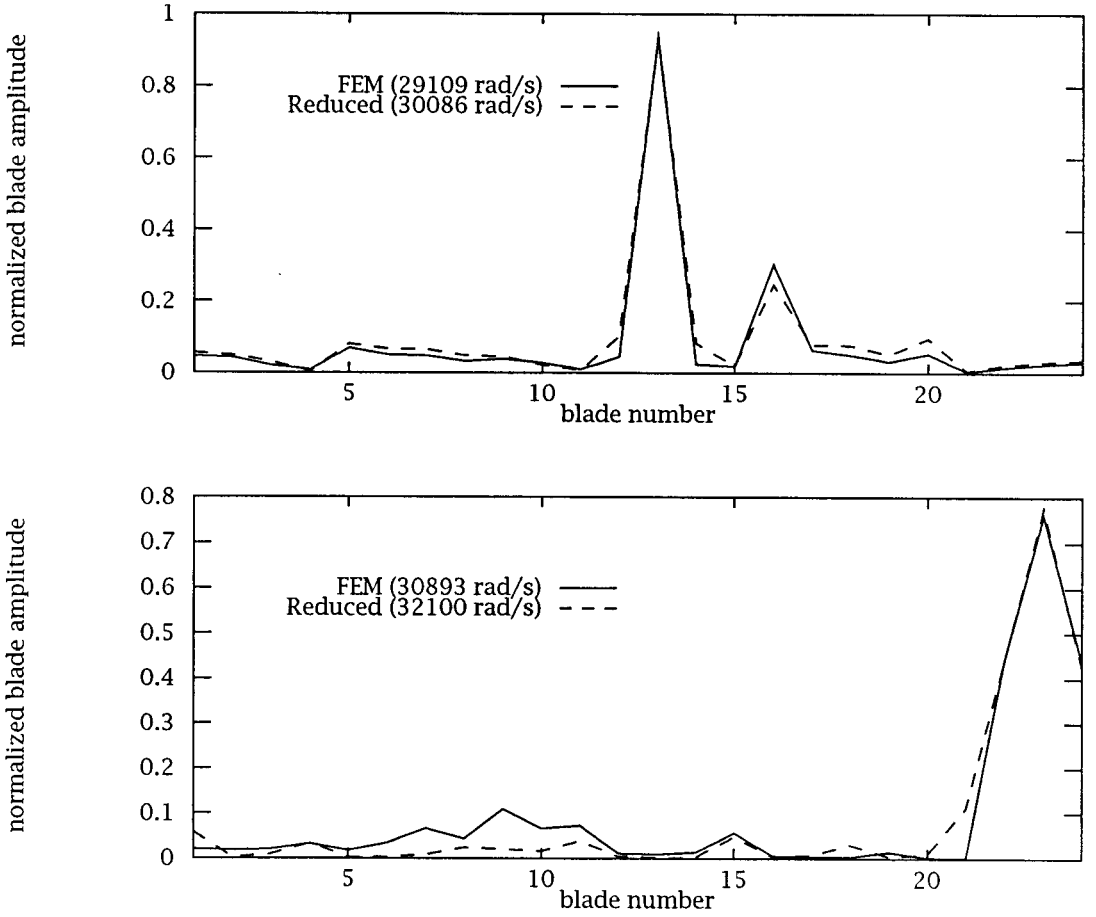

Figure 6 Selected localized mode shapes of a mistuned realization of the FEM compared with the ROM. Standard deviation of uniform mistuning is 5% .